THE UNIVERSITY OF WESTERN AUSTRALIA

Research Report of Intelligent Systems for Medicine Laboratory

Report # ISML/01/2013, January 2013

Non-linear finite element biomechanical model as a registration tool for image-guided neurosurgery: evaluation of accuracy against BSpline registration

Ahmed Mostayed, Revanth R. Garlapati, Aditi Roy, Grand R. Joldes, Adam Wittek, Karol Miller
Intelligent Systems for Medicine Laboratory
School of Mechanical and Chemical Engineering
The University of Western Australia
35 Stirling Highway
Crawley WA 6009, Australia
Phone: + (61) 8 6488 1901
Fax: + (61) 8 6488 1024
Email: mostayed@mech.uwa.edu.au
http://www.mech.uwa.edu.au/ISML/

Abstract

In this paper we evaluate the accuracy of warping of neuro-images using brain deformation predicted by means of patient-specific biomechanical model against the registration using BSpline-based free form deformation algorithm. Unlike the Bspline algorithm, biomechanics-based registration does not require a very expensive to acquire intra-operative MR image. Only sparse intra-operative data on the brain surface is sufficient to compute deformation for the whole brain. In this contribution the deformation fields obtained from both methods are qualitatively compared and overlaps of Canny edges extracted from the images are examined. We also define an edge based Hausdorff distance metric to quantitatively evaluate the accuracy of registration for these two algorithms. The qualitative and quantitative evaluations indicate that biomechanics-based registration algorithm, despite using much less input data, has higher registration accuracy than that of the BSpline algorithm.

Keywords: Non-rigid registration, Image-guided neurosurgery, Intra-operative MRI, Biomechanics, BSpline, Edge detection, Hausdorff distance, Evaluation of accuracy.

TABLE OF CONTENTS

1. Introduction

Our overall objective is to significantly improve the efficacy and efficiency of image-guided neurosurgery for brain tumours by incorporating realistic computation of brain deformations, based on a fully non-linear biomechanical model, in a system to improve intra-operative visualisation, navigation and monitoring. The system will create an augmented reality visualisation of the intra-operative configuration of the patient's brain merged with high resolution pre-operative imaging data, including functional magnetic resonance imaging and diffusion tensor imaging, in order to better localise the tumour and critical healthy tissues.

In this paper we are especially interested in image-guided surgery of cerebral gliomas. Neurosurgical resection is the primary therapeutic intervention in their treatment (Black, 1998). Near-total surgical removal is difficult due to the uncertainty in visual distinction of gliomatous tissue from adjacent healthy brain tissue. More complete tumour removal can be achieved through image-guided neurosurgery that uses intra-operative MRIs for improved visualization (Warfield, 2005). The efficiency of intra-operative visualization and monitoring can be significantly improved by fusing high resolution pre-operative imaging data with the intra-operative configuration of the patient's brain. This can be achieved by updating the pre-operative image to the current intra-operative configuration of the brain through registration. However, brain shift occurs during craniotomy (due to several factors including the loss of cerebrospinal fluid (CSF), changing pressure balances due to the impact of physiological factors and the effect of anaesthetics, and mechanical effects such as the impact of gravity on the brain tissue, and resection of tissue) and hence should be accounted for while registering the images.

Intra-operative MRI scanners are very expensive and often cumbersome. Hardware limitations of these scanners make it infeasible to achieve frequent whole brain imaging during surgery. The pre-

operative MRI must be updated frequently during the course of the surgical intervention as the brain is changing. An alternative approach is to acquire very rapid sparse intra-operative data and predict the deformation for the whole brain. To achieve this we developed a suite of algorithms based on brain tissue biomechanics for real-time estimation of the whole brain deformation from sparse intra-operative data (Joldes et al., 2010, Joldes et al., 2011).

The aim of this report is to demonstrate that our new algorithms, due to their utilisation of fundamental physics of brain deformation, and their efficient realisation in software, should enable at least as accurate registration of high quality pre-operative images onto the intra-operative position of the brain as is now possible with intra-operative MRI and state of the art non-rigid registration algorithm. We compare the accuracy of registration results obtained from two algorithms – (1) biomechanics-based Total Lagrangian Explicit dynamics (TLED) algorithm (Joldes et al., 2009b, Joldes et al., 2010, Joldes et al., 2011), that uses only the intra-operative position of the exposed surface of the brain; and (2) BSpline-based free form deformation (FFD) algorithm (Rueckert et al., 1999) as implemented in 3D Slicer, that uses an intra-operative MRI as a target image. We present results for thirteen neurosurgery cases that represent different situations which may occur during surgery as characterized by tumours located in different parts of the brain. The accuracy of these algorithms is compared qualitatively by viewing and exploring the calculated deformation fields and overlap of edges detected from MRI images. In addition, the registration error for each algorithm is also estimated quantitatively by means of a novel edge-based Hausdorff distance measure (Garlapati et al., 2012).

2. Methods

2.1. Non-rigid pre-operative to intra-operative registration using BSpline algorithm

Free form deformation (FFD) is a powerful tool for modelling 3D deformable objects and widely used in image morphing(Lee et al., 1995) and scattered data interpolation (Lee et al., 1997, Ruprecht and Muller, 1993). The basic idea of FFD is to deform an object by manipulating the underlying grid of control points (Rueckert et al., 1999). In order to smoothly propagate the user specified values at the control points throughout the domain of the image, a BSpline based FFD algorithm was proposed by Lee et al.(Lee et al., 1997) The BSpline algorithm was later adapted by (Rueckert et al., 1999) for non-rigid registration of medical images. Since then the BSpline algorithm has become one of the most widely used non-rigid registration algorithm for medical images (Kybic et al., 2000, Kybic and Unser, 2003, Rohlfing et al., 2003, Schnabel et al., 2001).

The basic components of an image-based registration algorithm (Hill and Batchelor, 2001), used also by BSpline–based methods, are presented in **Fig. 1**. The moving (pre-operative) image (**M**) is transformed using the chosen transformation **T** (in this case the displacements of control points) to obtain the transformed image **T(M)**. The transformed image is then compared with the fixed (intra-operative) image (**F**) based on a chosen similarity measure **S**. This similarity metric is used by an optimizer to find the parameters of the transform that minimizes the difference between the moving and fixed image. An optimization loop is therefore required, which changes the transform parameters to find the best agreement between the fixed and moving image.

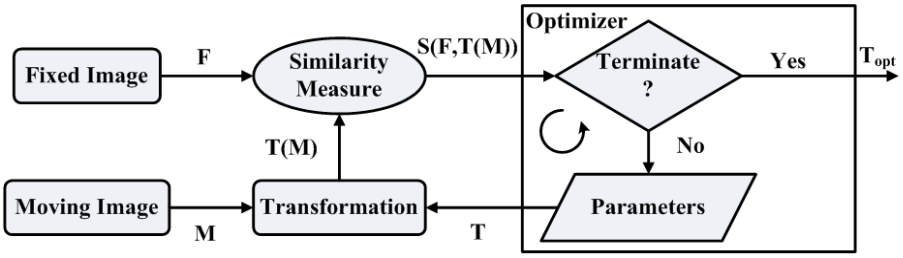

Figure 1. Basic components of a general image based registration process.

Below the implementation of this algorithm in 3D Slicer is described briefly. A number of factors influencing the registration results for image guided-neurosurgery are also discussed in the following subsection.

Estimation of probability densities: The most commonly used similarity measure ($C_{similarity}$) in multi-modal non-rigid registration is mutual information. Calculation of mutual information between the target and the transformed source image requires the values of the marginal and joint probability densities (PDF) of image intensities. These probability densities are usually not readily known; therefore they must be estimated from discrete image data. In 3D Slicer the probability densities are estimated using Parzen windows (Thevenaz and Unser, 1997). In this scheme, the densities are constructed by taking limited number of intensity samples S_i from the images and super-imposing a kernel function K centred on S_i.

Implementation of similarity measure: The similarity measure used in 3D Slicer BSpline registration module is the definition of mutual information used in (Mattes et al., 2001). In this implementation, the joint and marginal probability densities are estimated from a set of intensity samples drawn from the images. A zero-order BSpline kernel is used to estimate the PDF of the target image intensities. On the other hand, cubic BSpline kernel is used to estimate the source image PDF (Mattes et al., 2003).

2.1.1 BSpline registration for image-guided neurosurgery

In the case of image-guided neurosurgery where the pre-operative image is required to be registered with the intra-operative (after craniotomy is performed) image, the Bspline registration algorithm faces a number of challenges. First of all, the large difference in intensities between the pre-operative and intra-operative MRI often influences the registration result. Intensity normalization between the source and target image is required to achieve decent registration results. Secondly, the presence of skull in the intra-operative image makes the registration process difficult and can induce large error in the registration of soft tissues. In order to achieve good alignment skull must be stripped from both the pre- and intra-operative images. In addition, setting an appropriate set of parameters (density of control point grid, number of spatial samples and number of histogram bins) for a particular registration case requires expert knowledge. Without performing proper pre-processing steps and appropriate parameter setting it is extremely difficult to obtain reasonable results from a BSpline registration algorithm. We carried out a single study to find the effects of the pre-processing steps on the registration results as well as to select the appropriate control point mesh density. Effect of these factors on the quality of registration is demonstrated below on a patient-specific case.

Effect of skull stripping: Fig. 2 shows the effect of skull stripping (through segmentation) on the registration result. When no stripping is performed (**Fig. 2a**), large misalignment between the intra-operative and registered pre-operative brain contours can be observed. However, the contours of the ventricles show higher degree of alignment. On the other hand when stripping is performed (**Fig. 2b**), the misalignment between brain contours decreases but the misalignment between ventricle contours increases. It is an indication that the BSpline registration favours larger anatomical regions (brain parenchyma) over smaller regions (ventricles and tumours).

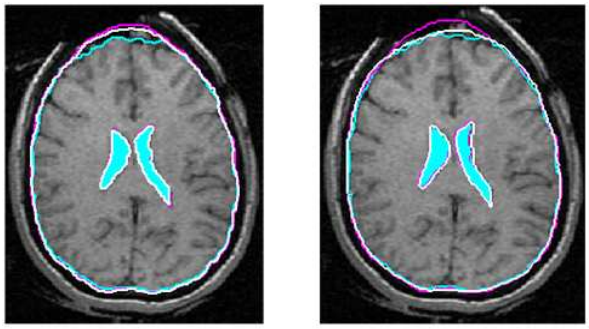

(a) (b)

Figure 2. Effect of skull segmentation on registration result: (a) Before skull segmentation and (b) After skull degmentation. The intra-operative and pre-operative contours are overlayed on the intra-operative axial slice. Colour codes: Light blue shade – ventricles in the intra-operative image; Light blue contour – outline of parenchyma in the intra-operative image; Majenta contours – outlines of parenchyma and ventricles in the pre-operative image before registration; White contours - outlines of parenchyma and ventricles in the pre-operative image after registration. 50000 spatial samples and a 10 x 10 x 10 control point grid is used for both cases.

Effect of control point mesh density: Fig. 3 shows the effect of control point mesh density on registration result. As the control point mesh density is increased, the alignment of brain contours improves but the alignment of ventricle contours decreases. At a 20 x 20 x 20 control grid (**Fig. 3c**) the alignment of brain contours is very good, but the alignment of ventricles is very poor. This result again indicates the bias of the registration algorithm towards larger anatomic regions. We concluded that a 10 x 10 x 10 control point grid yields best results.

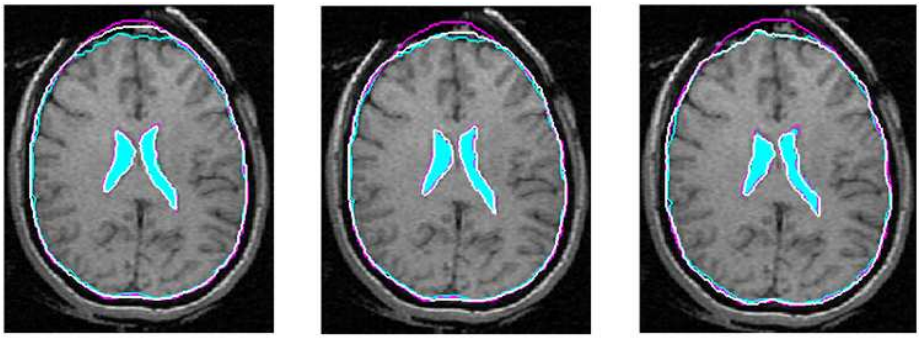

Figure 3. Effect of control point mesh density on registration result: (a) Mesh Density 5 x 5 x 5, (b) Mesh Density 10 x 10 x 10 and (c) Mesh Density 20 x 20 x 20. The intra-operative and pre-operative contours are overlayed on the intra-operative axial slice. Colour codes: Light blue shade – ventricles in the intra-operative image; Light blue contour – outline of parenchyma in the intra-operative image; Majenta contours – outlines of parenchyma and ventricles in the pre-operative image before registration; White contours - outlines of parenchyma and ventricles in the pre-operative image after registration. In all three cases skulls are stripped. 50000 spatial samples are used for all three cases.

Effect of intensity normalization: In this pre-processing step the intensity of the images were normalized by N4 algorithm(Tustison et al., 2010) for bias field correction followed by histogram equalization. Although intensity normalization does not affect the alignment of brain contours much, it significantly improves the alignment of the ventricle contours (**Fig. 4b**).

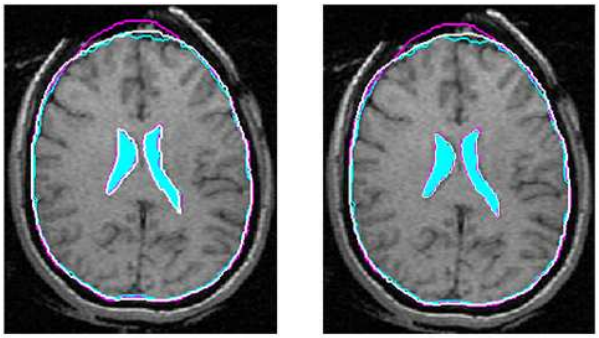

(a) (b)

Figure 4. Effect of intensity normalization on registration result: (a) and (b). The intra-operative and pre-operative contours are overlayed on the intra-operative axial slice. Colour codes: Light blue shade – ventricles in the intra-operative image; Light blue contour – outline of parenchyma in the intra-operative image; Majenta contours – outlines of parenchyma and ventricles in the pre-operative image before registration; White contours - outlines of parenchyma and ventricles in the pre-operative image after registration. In both cases skulls are stripped. 50000 spatial samples and 10 x 10 x 10 control grid are used for both cases.

2.2. Biomechanics-based prediction of deformations using only the information of the exposed brain surface

Unlike the BSpline registration algorithm, biomechanics-based registration methods do not require an intra-opearive image to update the pre-operative image (see **Fig. 5**). The pre-operative image is segmented first to extract the antomical features of interest. Based on this segmentation (which can be acquired days before the surgery) a computational grid (mesh) is generated. A biomechanical model further is defined by incorporating boundary conditions (contact between skull and brain for example) and material properties for each tissue types. The model is completed by defining the loading conditions. This loading informations are generally obtained from sparse intra-operative information

(such as surface deformation at the area of craniotomy). Once the model is constructed, a solver (finite element or meshless) is used to compute the transform, which is then applied to warp the pre-operative image. The warping procedure requires the mapping of points in the moving (pre-operative) image to new locations in the transformed image. The intensity of the points in the transformed image is determined by interpolating intensities of the corresponding points in the moving image. In the following subsections the non-linear finite element algorithm proposed by Joldes et al (Joldes et al., 2009b) to predict the intra-operative brain shift is briefly described.

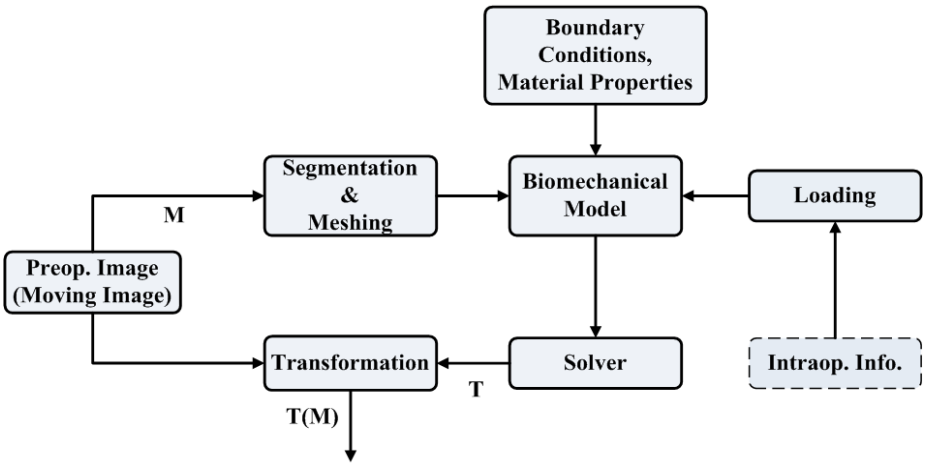

Figure 5. Registration process based on a biomechanical model.

2.2.1. Construction of finite element mesh for patient-specific brain models

A three dimensional (3D) surface model of each patient's brain was created from segmented pre-operative magnetic resonance image (MRI). The segmentation was done using the region growing algorithm implemented in 3D slicer. The meshes were constructed using low-order elements (linear tetrahedron or hexahedron) to meet the computation time requirement. To prevent volumetric locking the tetrahedral elements with average nodal pressure (ANP) formulation (Joldes et al., 2009d) was

used. The meshes were generated using IA-FEMesh (Grosland et al., 2009) and HyperMesh (commercial FE mesh generator by Altair of Troy, MI, USA). A typical mesh (Case 1) is shown in **Fig. 6**. This mesh consists of 14447 hexahedral elements, 13563 tetrahedral elements and 18806 nodes. Each node in the mesh has three degrees of freedom.

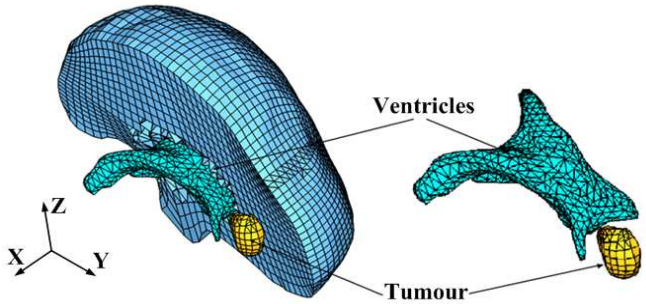

Figure 6. Typical example (Case 1) of a patient-specific mesh built for this study.

2.2.2. Displacement loading

The models were loaded by prescribing displacements on the exposed part (due to craniotomy) of the brain surface. At first the pre-operative and intra-operative coordinate systems were aligned by rigid registration. Then the displacements at the mesh nodes located in the craniotomy region were estimated with the interpolation algorithm we described in previous publication (Joldes, 2009d).

2.2.3 Boundary conditions

The stiffness of the skull is several orders of magnitude higher than that of the brain tissue. Therefore**,** in order to define the boundary conditions for the unexposed nodes of the brain mesh, a contact interface (Joldes et al., 2008d) was defined between the rigid skull model and the deformable brain. The interaction was formulated as a finite sliding, frictionless contact between the brain and the skull. This contact formulation prevents the brain surface form penetrating the skull by checking the nodes of the brain mesh for penetration (Joldes et al., 2008d).

2.2.4. Mechanical properties of the intracranial constituents

If geometric non-linearity is considered (Wittek et al., 2009), the predicted deformation field within the brain is only weakly affected by the constitutive model of the brain tissue. Therefore, for simplicity a hyper-elastic Neo-Hookean model was used (Joldes et al., 2009a). The Young's modulus of 3000 Pa was selected for parenchyma (Miller and Chinzei, 2002). The Young's modulus for tumour was assigned two times larger than that for parenchyma, keeping it consistent with the experimental data of (Sinkus et al., 2005). As the brain tissue is almost incompressible, Poisson's ratio 0.49 was chosen for the parenchyma and tumour (Wittek et al., 2007). Following (Wittek et al., 2007) The ventricles were assigned properties of a very soft compressible elastic solid with Young's modulus of 10 Pa and Poisson's ratio of 0.1.

2.2.5. Solution algorithm

An efficient algorithm for integrating the equations of solid mechanics has been developed by Joldes et al (Miller et al., 2007). The computational efficiency of this algorithm is achieved by using - 1) Total Lagrangian (TL) formulation (Miller et al., 2007) for updating the calculated variables; and 2) Explicit Integration in the time domain combined with mass proportional damping. In the TL formulation, all the calculated variables (such as displacements and strains) are referred to the original configuration of the analyzed continuum (Joldes et al., 2009c). The decisive advantage of this formulation is that all derivatives with respect to spatial coordinates can be pre-computed. The Total Lagrangian formulation also leads to a simplification of material law implementation as these material models can be easily described using the deformation gradient (Joldes et al., 2009b).

The integration of equilibrium equations in time domain was performed using explicit method. In explicit time integration, the displacement at time $t+\Delta t$ (where Δt is the time step) is solely based on the equilibrium at time t. Therefore, no matrix inversion and iterations are required when solving

nonlinear problems. Application of explicit time integration scheme reduces the time required to compute the brain deformations by two orders of magnitude in comparison to implicit integration typically used in commercial finite element codes like ABAQUS (ABAQUS, 1998). This algorithm is also implemented in GPU (NVIDIA Tesla C1060 installed on a PC with Intel Core2 Quad CPU) for real-time computation (Joldes et al., 2010) so that the entire model solution takes less than four seconds on a commodity hardware.

2.3. Methods for evaluation of registration accuracy

2.3.1. Qualitative evaluation

Deformation field: The physical plausibility of the registration results are verified by examining the computed displacement vector at each voxel of the pre-operative image domain. The deformations are computed at voxel centres only for a region of interest near the tumour.

Overlap of edges: To obtain a qualitative assessment of the degree of alignment after registration, one must examine the overlap of corresponding anatomical features of the intra-operative and registered pre-operative image. For this purpose, tumours and ventricles in both registered pre-operative and intra-operative images can be segmented and their surfaces can be compared (Wittek et al., 2010). Image segmentation is time consuming, not fully automated and not suitable for comparing a large number of image pairs (Fedorov et al., 2008). Therefore in this paper Canny edges (Canny, 1986) are used as feature points. Edges are regarded as useful and easily recognizable features, and they can be detected using techniques that are automated and fast. Canny edges obtained from the intra-operative and registered pre-operative image slices are labelled in different colours and overlaid (as shown in **Section 3.1.2**).

2.3.2. Quantitative evaluation

Edge-based Hausdorff distance: The Hausdorff distance is a popular measure to calculate similarities between two images (Huttenlocher, 1993). It is defined to compare two sets of feature points **A** and **B** . We begin with a definition of the traditional point-based Hausdorff distance (HD) between two intensity images **I** and **J**. Let *I* and *J* be the binary edge images derived from **I** and **J** respectively, and $\mathbf{A} = \{a_1, \cdots, a_n\}$ and $\mathbf{B} = \{b_1, \cdots, b_n\}$ are the set of non-zero points corresponding to the non-zero pixels on the edge images. The directed distance between them $h(\mathbf{A}, \mathbf{B})$ is defined as the maximum distance from any of the points in the first set to the second one:

$$h(\mathbf{A}, \mathbf{B}) = \underset{a \in \mathbf{A}}{\operatorname{argmax}} \left[\underset{b \in \mathbf{B}}{\operatorname{argmin}} \| a - b \|_2 \right] \qquad (1)$$

$$h(\mathbf{B}, \mathbf{A}) = \underset{b \in \mathbf{B}}{\operatorname{argmax}} \left[\underset{a \in \mathbf{A}}{\operatorname{argmin}} \| b - a \|_2 \right] \qquad (2)$$

The HD between the two sets $H(\mathbf{A}, \mathbf{B})$ is defined as the maximum of these two directed distances:

$$H(\mathbf{A}, \mathbf{B}) = \max(h(\mathbf{A}, \mathbf{B}), h(\mathbf{B}, \mathbf{A})) \qquad (3)$$

Several improvements of the directed distance have been proposed (Zhao et al., 2005). One of them is the percentile Hausdorff distance, which is very useful to delete outliers, and the directed distance is defined as:

$$h_{\mathrm{P}}(\mathbf{A}, \mathbf{B}) = \underset{a \in \mathbf{A}}{\mathrm{P}^{\mathrm{th}}} \left[\underset{b \in \mathbf{B}}{\operatorname{argmin}} \| a - b \|_2 \right] \qquad (4)$$

where P is the P^{th} percentile of $\left[\underset{b \in \mathbf{B}}{\operatorname{argmin}} \| a - b \|_2 \right]$.

The above definition of Hausdorff distance sets an upper-limit on the dissimilarities between two images. It implies that the value indicated by **Eq. 3** generally comes from a single pair of points.

The other point pairs have a distance less than or equal to that value. Such a measure is very useful for template based image matching. However, while measuring the misalignments between two medical images, it is desirable to calculate the distance between local features (in the case of brain MRI contour lines of tumour, ventricles etc.) in two images that correspond to each other. To calculate such a distance we define the edge-based Hausdorff distance.

We define directed distance between two sets of edges as

$$h_e(\mathbf{A}^e, \mathbf{B}^e) = \underset{a_i^e \in \mathbf{A}^e}{\operatorname{argmax}} \left[\underset{b_j^e \in \mathbf{B}^e}{\operatorname{argmin}} \left\| a_i^e - b_j^e \right\| \right] \qquad (5)$$

where $\mathbf{A}^e = \{a_1^e, \cdots, a_m^e\}$ and $\mathbf{B}^e = \{b_1^e, \cdots, b_n^e\}$ are two sets of edges.

The quantity $\left\| a_i^e - b_j^e \right\|$ in **Eq. 5** is nothing but the point based Hausdorff distance between two point sets $\mathbf{M} = \{m_1, \cdots, m_p\}$ and $\mathbf{T} = \{t_1, \cdots, t_q\}$ representing edges a_i^e and b_i^e respectively,

$$\left\| a_i^e - b_j^e \right\| := d(a_i^e - b_j^e) = \max\left(h(\mathbf{T}, \mathbf{M}), h(\mathbf{M}, \mathbf{T})\right) \qquad (6)$$

Now the edge-based Hausdorff Distance is defined as

$$H_e(\mathbf{A}^e, \mathbf{B}^e) = \max\left(h_e(\mathbf{A}^e, \mathbf{B}^e), h_e(\mathbf{B}^e, \mathbf{A}^e)\right) \qquad (7)$$

Similar to the percentile point-based Hausdorff distance, one can construct a percentile edge-based Hausdorff distance:

$$h_{\mathrm{P}_e}(\mathbf{A}^e, \mathbf{B}^e) = \underset{a_i^e \in \mathbf{A}^e}{\mathrm{P}^{\mathrm{th}}} \left[\underset{b_j^e \in \mathbf{B}^e}{\operatorname{argmin}} \left\| a_i^e - b_j^e \right\| \right] \qquad (8)$$

This percentile edge-based Hausdorff distance (**Eq. 8**) is not only useful for removing outlier edge-pairs, but also can be interpreted in a different way. The P^{th} percentile Hausdorff distance, 'D', between two images means that 'P' percent of total edge pairs have a Hausdorff distance below D. Therefore, instead of reporting only one Hausdorff distance value (using **Eq. 7**), **Eq. 8** can be used to

report Hausdorff distance values for different percentiles. A plot of the Hausdorff distance values at different percentiles (see **Section 3.2**) immediately reveals the percent of edges that have misalignments below an acceptable error.

In order to obtain those curves of Hausdorff distance values at different percentiles, each image volume was cropped into a region-of-interest (ROI) which encloses the tumour (as mentioned in the previous section). These ROI sub-volumes were then super-sampled (0.5 mm x 0.5 mm x 0.5 mm) to obtain isotropic voxels. This was done to improve the precision of Canny edge detection(Canny, 1986) used in the registration accuracy evaluation process. The sub-volumes were also re-sliced along the sagittal plane in an effort to capture misalignments in a direction orthogonal to the axial slices. Then the edge-based Hausdorff distance (HD) was used to calculate the misalignment between slices along both axial and sagittal directions. The directed distances for all edge pairs (see **Eq. 6**) were recorded and the edge-based Hausdorff distance values at different percentile of directed distances were plotted.

Pre-processing - Outlier Removal: Although edges are supposed to be representative of consistent features present in two separate images, outliers are very common if the intensity ranges of the images are different. It is often the case in multi-modal image registration. Therefore, pre-processing of the extracted edges is required to remove outliers before the edge-based Hausdorff distance could be calculated. We used a pre-processing step (Garlapati et al., 2012), called the “round-trip consistency” procedure that removes the pixels of one image that do not correspond to the other image.

3. Results

3.1. Qualitative evaluation of registration results

3.1.1 Deformation field

The deformation fields predicted by the biomechanical model and obtained from the BSpline transform are compared in **Fig. 7**. These deformation fields are three dimensional. However, for clarity, only arrows representing 2D vectors (x and y component of displacement) are shown overlaid on undeformed pre-operative slices. Each of these arrows represents the displacement of a voxel of the pre-operative image domain. In general the displacements fields calculated by the BSpline registration algorithm are similar to the predicted displacements by the biomechanical model at the outer surface of the brain. But in the interior of the brain volume the displacements vectors differ in both magnitude and direction. In three of the cases (cases 8, 11 and 12) the difference in the displacement fields is smaller compared to the other cases.

3.1.2. Overlap of Canny edges

From **Fig. 8** we can see that misalignments between the edges detected from the intra-operative images and the edges from the pre-operative images updated to the intra-operative brain geometry are much lower for the biomechanics-based warping than for BSpline registration. The edges obtained from the images warped with both registration algorithms have higher similarity for cases 8, 11 and 12 than the other cases. It is due to the fact that the deformation fields predicted using the biomechanical model and BSpline registration have higher similarity for these three cases. For instance, large misalignments between the edges obtained from the intra-operative image and edges from the pre-operative image registered using BSpline algorithm can be observed for Case 2. For this case there was a large intra-

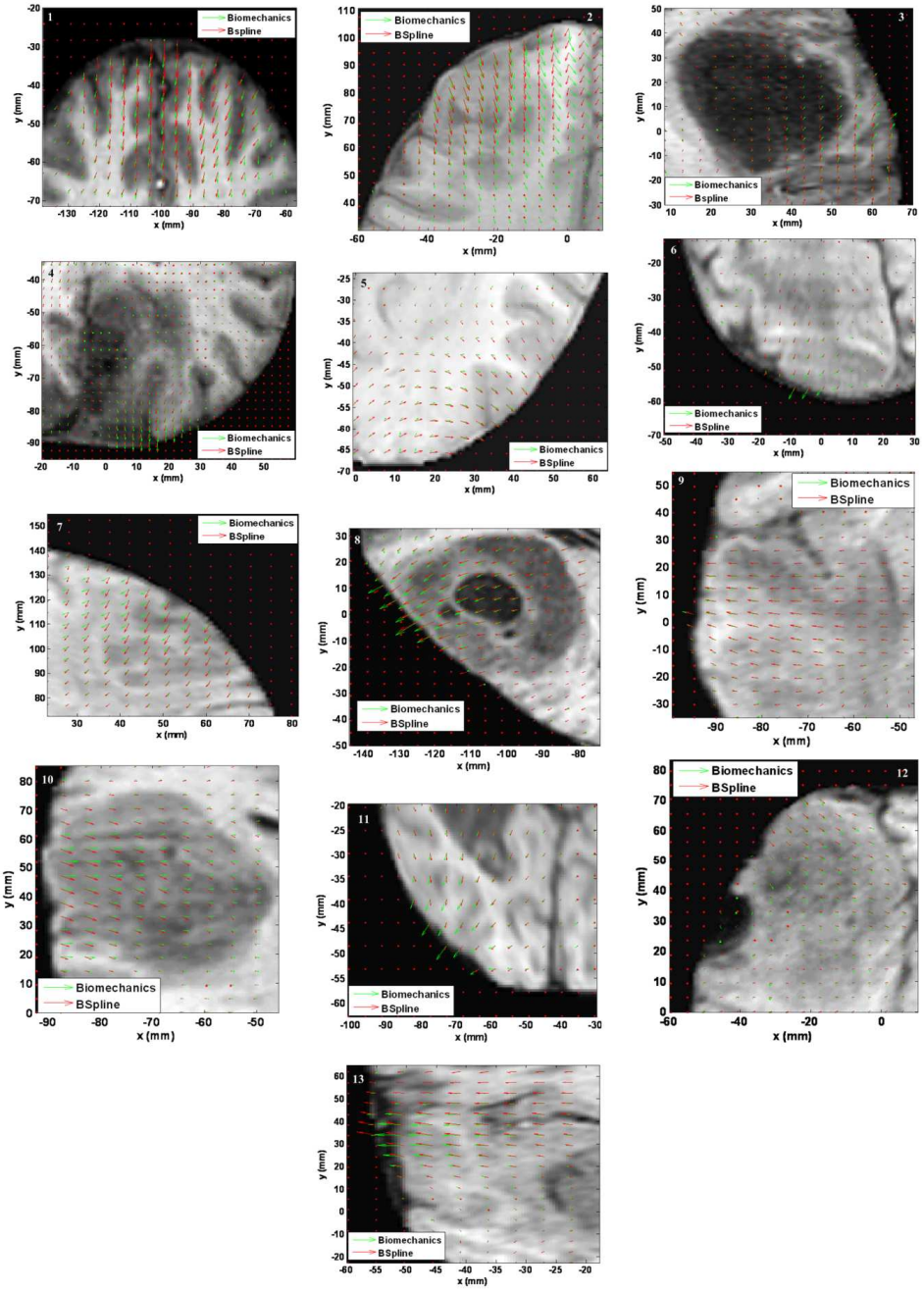

Figure 7. The predicted deformation fields overlaid on an axial slice of pre-operative image. An arrow represents a 2D vector consisting of the x (R-L) and y (A-P) components of displacement at a voxel centre. Green arrows: deformation field predicted by biomechanical model. Red arrows: deformation field calculated by BSpline algorithm. The number on each image denotes a particular neurosurgery case.

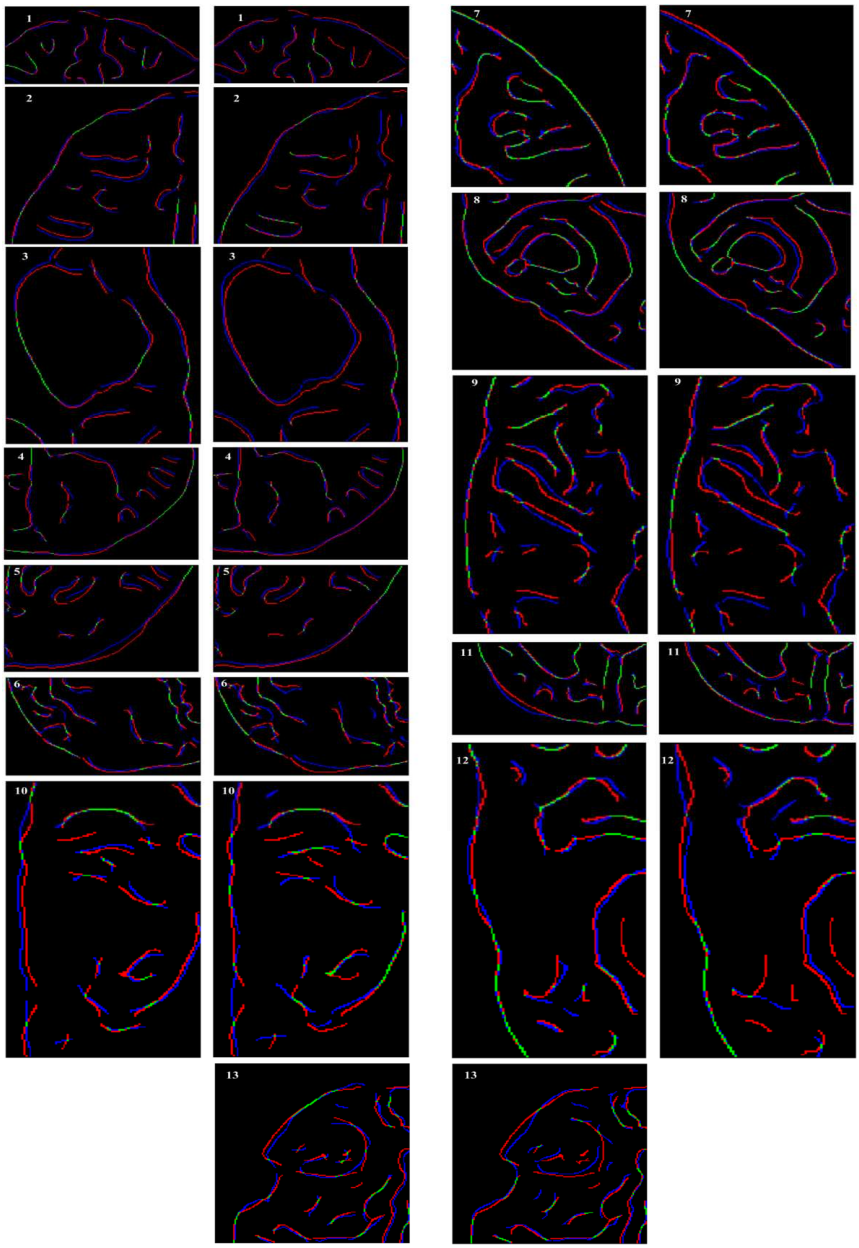

Figure 8. Canny edges extracted from intra-operative and the registered pre-operative image slices overlaid on each other. Red colour represents the non-overlapping pixels of the intra-operative slice and blue colour represents the non-overlapping pixels of the pre-operative slice. Green colour represents the overlapping pixels. The number on each image denotes a particular neurosurgery case. For each case, the left image shows edges for the biomechanics-based warping and the right image shows edges for the BSpline-based registration.

operative brain shift (8mm) and the deformation field obtained using BSpline algorithm significantly differs from deformation predicted using biomechanical model. It is an indication that the biomechanics-based warping may perform more reliably than the BSpline registration algorithm if large deformations are involved.

3.2. Quantitative evaluation of registration results

The percentile vs. Hausdorff distance (HD) curve provides an estimation of the percentage of edges that were successfully registered in the registration process. As accuracy of the edge detection is limited within the image resolution, an alignment error smaller than two times the original in-plane resolution of the intra-operative image (which is 0.8594 mm for the thirteen cases considered) is difficult to avoid. Hence, for thirteen clinical cases analyzed here, we considered any edge pair having HD value less than 1.7 mm be successfully registered. It is obvious from **Fig. 9** and **10** that biomechanical warping was able to successfully register more edges than the BSpline registration for all thirteen cases.

Percentiles of edges successfully registered by two registration algorithms (i.e. warping using biomechanical model and BSpline registration) for each analyzed case are listed in **Table 1**. The percentile of successfully registered edge is slightly higher for image warping using biomechanical model than that for BSpline registration (with an exception for Case 7). It can be noted that the Hausdorff distance values in the sagittal plane are generally higher than those in the axial plane. This is most likely caused by the interpolation artefact (due to the poor resolution in the sagittal plane) introduced in the re-slicing process.

For all thirteen cases, the percentiles vs. HD curves tend to rise steeply around 90 percentile. Hence, it can be safely assumed that most edge pairs that lie between 91 and 100 percentile do not have

any correspondence (possible outliers). The 90-percentile HD values for five cases are listed in **Table 2**.

Table 1. Percentile of edges successfully registered for thirteen patient specific cases.

Case	Percentile of edges successfully registered			
	Axial Slices		Sagittal Slices	
	Biomechanics	BSpline	Biomechanics	BSpline
'1'	70	63	61	47
'2'	56	45	38	41
'3'	54	29	54	33
'4'	66	54	67	46
'5'	58	45	54	33
'6'	59	51	58	53
'7'	75	81	61	76
'8'	75	70	69	65
'9'	52	43	52	46
'10'	61	55	61	57
'11'	82	77	81	62
'12'	63	59	58	60
'13'	81	67	82	62

Table 2. 90 percentile Hausdorff distance values for five patient specific cases.

Case	Non-rigid registration algorithm			
	Axial Slices		Sagittal Slices	
	Biomechanics	BSpline	Biomechanics	BSPline
'1'	2.43 mm	2.75 mm	2.75 mm	3.54 mm
'2'	2.43 mm	3.36 mm	2.72 mm	3.87 mm
'3'	2.19 mm	3.10 mm	2.43 mm	3.44 mm
'4'	2.15 mm	2.75 mm	2.15 mm	2.61 mm
'5'	2.58 mm	3.36 mm	2.58 mm	3.87 mm
'6'	3.14 mm	3.44 mm	3.32 mm	3.75 mm
'7'	2.34 mm	2.15 mm	2.39 mm	2.34 mm
'8'	2.34 mm	2.73 mm	2.34 mm	2.96 mm
'9'	3.00 mm	4.03 mm	3.66 mm	4.32 mm
'10'	2.73 mm	3.14 mm	2.85 mm	3.41 mm
'11'	1.99 mm	2.52 mm	2.10 mm	2.65 mm
'12'	2.81 mm	3.28 mm	3.14 mm	3.78 mm
'13'	1.99 mm	2.85 mm	1.99 mm	2.65 mm

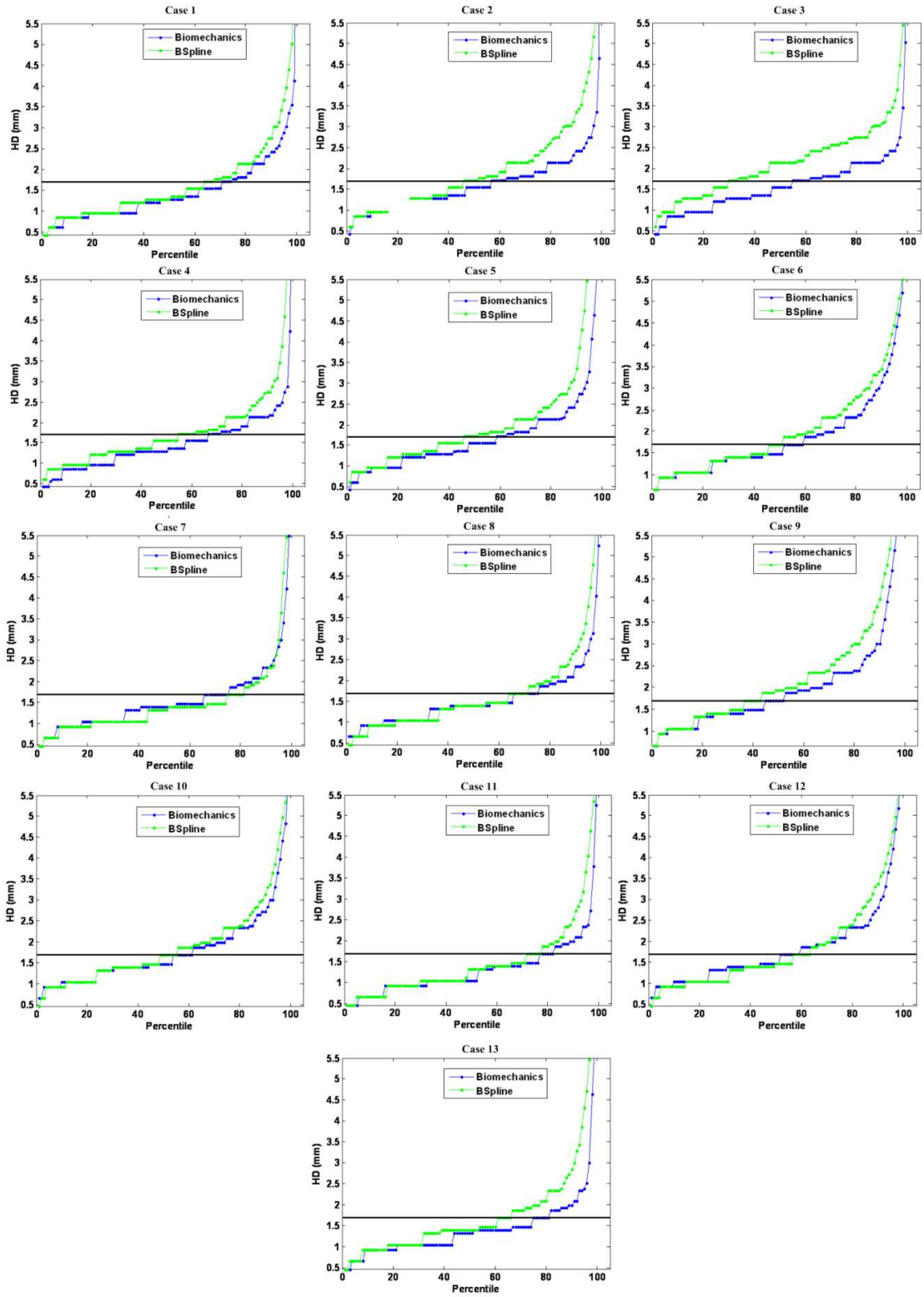

Figure 9. The plot of Hausdorff distance between intra-operative and registered pre-operative images against the percentile of edges for axial slices. The horizontal line is the 1.7 mm mark.

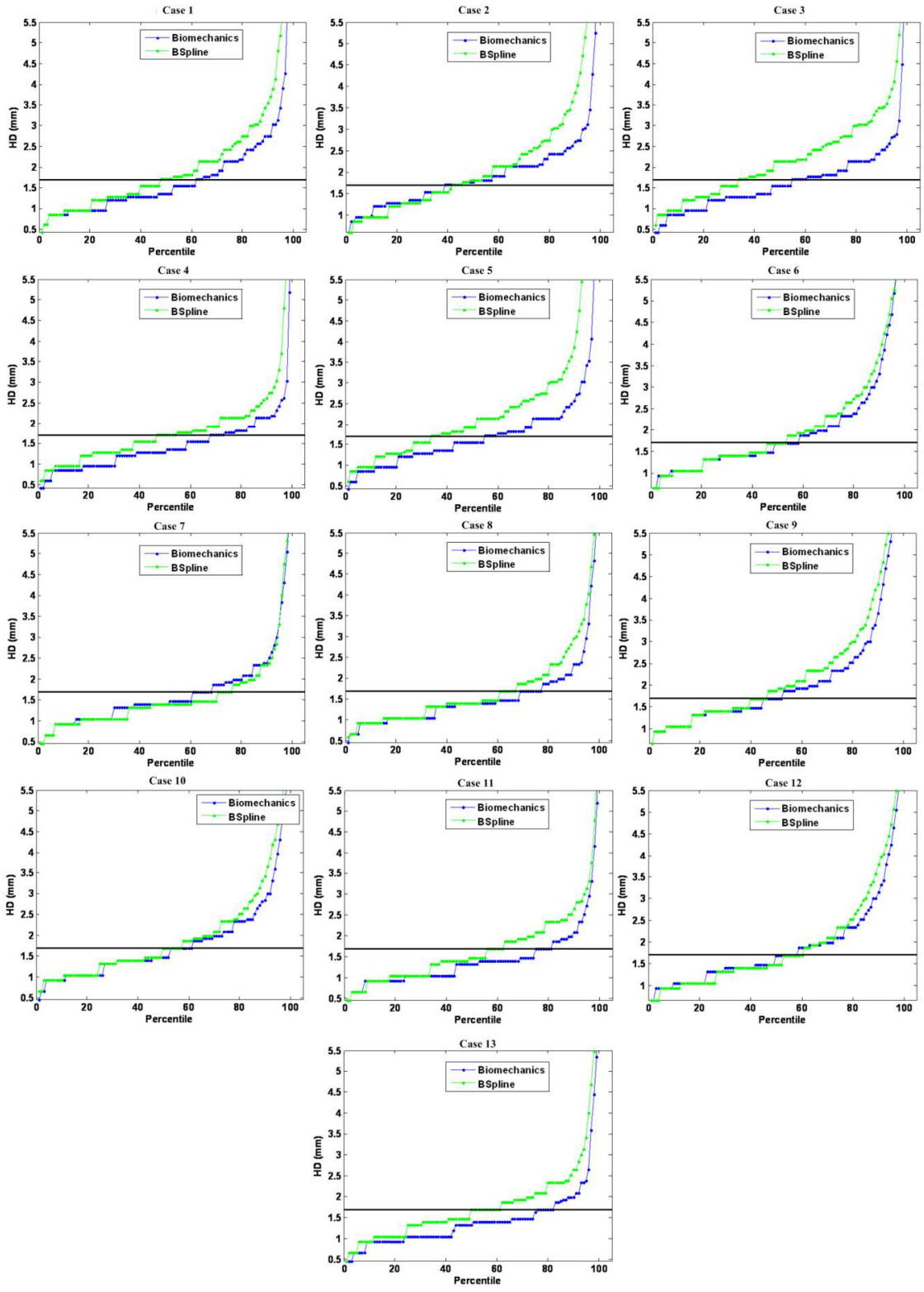

Figure 10. The plot of Hausdorff distance between intra-operative and registered pre-operative images against the percentile of edges for sagittal slices. The horizontal line is the 1.7 mm mark.

4. Discussions

From the results presented in Section 3 it is evident that application of the intra-operative deformation predicted using patient-specific biomechanical model (Wittek et al., 2010) to warp pre-operative images ensures slightly higher registration accuracy than that of 3D Slicer BSpline registration module. Biomechanical models are especially effective in neurosurgery cases where intra-operative brain shift is large (Case 2 for instance). Another distinctive advantage of the biomechanical algorithm is that it does not need the intra-operative image at all to compute deformation. Only the displacement of a limited number of points on the exposed (during craniotomy) intra-operative brain surface is required. Such displacement can be determined from 3D ultrasound or 3D laser range imaging (Ji et al., 2011), or even measured during the surgery using a tracked pointer tool available e.g. within the Stealth system (Medtronic, 2010), with which the surgeon can touch a number of points on the brain surface. For image warping using the intra-operative brain deformation predicted from patient-specific biomechanical model, the required amount of intra-operative data points is reduced by four orders of magnitude compared to BSpline registration (see **Table 3**).

Table 3. Number of points of intra-operative geometry required for numerical computation.

Case	Data Requirement (No. of points)	
	Biomechanics	BSpline
'1'	322	3.932×10^6
'2'	328	3.932×10^6
'3'	171	3.932×10^6
'4'	134	3.932×10^6
'5'	63	3.932×10^6
'6'	228	3.932×10^6
'7'	348	3.932×10^6
'8'	511	3.932×10^6
'9'	223	3.932×10^6
'10'	363	3.932×10^6
'11'	276	3.932×10^6
'12'	312	3.932×10^6
'13'	138	3.932×10^6

We chose widely used BSpline implementation available in 3D Slicer. It may be argued that better implementations exist. However, without a doubt 3D Slicer's implementation is widely used and considered reliable. To strengthen the conclusions of this work an alternative implementation and alternative algorithms for image-based alignment should be evaluated in future work.

We believe that the results presented in this paper have the potential to significantly advance the way imaging is used to guide the resection of brain tumours. Presently, our experience has demonstrated the great utility of intra-operative MRI in ensuring complete resection, particularly of low grade tumours. However, this often comes at the expense of significantly longer operating times, as well as being resource intense. For example, the decision to acquire a new volumetric image requires expertise from technologists, radiologists, and others. At hospitals that have at their disposal the intra-operative MRI, the ability to know when imaging is needed, as well as the potential reduction in the number of imaging acquisitions promises to make intra-operative MRI a much more effective and efficient technique.

Even more importantly, we believe that the use of comprehensive biomechanical computations in the operating theatre may present a viable and economical alternative to intra-operative MRI. The brain deformation modelling algorithms proposed here may lead the way towards allowing updated representations of the brain position even without intra-operative MRI and therefore bring the success of image-guided neurosurgery to much wider population of sufferers.

Acknowledgements: The first author is a recipient of the SIRF scholarship and acknowledges the financial support of the University of Western Australia. The financial support of National Health and Medical Research Council (Grant No. APP1006031) is gratefully acknowledged. This investigation was also supported in part by NIH grants R01 EB008015 and R01 LM010033, and by a research grant from the Children's Hospital Boston Translational Research Program. In addition, the authors also gratefully acknowledge the financial support of Neuroimage Analysis Center (NIH P41 EB015902), National Center for Image Guided Therapy (NIH U41RR019703) and the National Alliance for Medical Image Computing (NAMIC), funded by the National Institutes of Health through the NIH Roadmap for Medical Research, Grant U54 EB005149. Information on the National Centers for Biomedical Computing can be obtained from http://nihroadmap.nih.gov/bioinformatics.

REFERENCES

3D Slicer. http://www.slicer.org.

ABAQUS 1998. *ABAQUS Theory Manual. Version 5.8,* Hibbitt, Karlsson & Sorensen, Inc.

BLACK, P. 1998. Management of malignant glioma: role of surgery in relation to multimodality therapy. *J Neurovirol,* 4**,** 227-36.

CANNY, J. 1986. A Computational Approach to Edge Detection. *Pattern Analysis and Machine Intelligence, IEEE Transactions on,* PAMI-8**,** 679-698.

FEDOROV, A., BILLET, E., PRASTAWA, M., GERIG, G., RADMANESH, A., WARFIELD, S. K., KIKINIS, R. & CHRISOCHOIDES, N. 2008. Evaluation of Brain MRI Alignment with the Robust Hausdorff Distance Measures. *Proceedings of the 4th International Symposium on Advances in Visual Computing.* Las Vegas, NV: Springer-Verlag.

GARLAPATI, R. R., JOLDES, G. R., WITTEK, A., LAM, J., WEISENFIELD, N., HANS, A., WARFIELD, S. K., KIKINIS, R. & MILLER, K. Year. Objective evaluation of accuracy of intra-operative neuroimage registration. *In:* Computational Biomechanics for Medicine XII (MICCAI 2012 Associated Workshop), 2012 Nice, France. Springer.

GROSLAND, N. M., SHIVANNA, K. H., MAGNOTTA, V. A., KALLEMEYN, N. A., DEVRIES, N. A., TADEPALLI, S. C. & LISLE, C. 2009. IA-FEMesh: An open-source, interactive, multiblock approach to anatomic finite element model development. *Comput. Methods Prog. Biomed.,* 94**,** 96-107.

HILL, D. L. G. & BATCHELOR, P. 2001. Registration Methodology: Concepts and Algorithms *In:* HANJAL, J. V., HILL, D. L. G. & HAWKES, D. J. (eds.) *Medical image registration.* CRC press.

HUTTENLOCHER, D. P. 1993. Comparing images using the Hausdorff distance *IEEE Transactions on Pattern Analysis and Machine Intelligence,* 15**,** 850-853.

JI, S., FAN, X., ROBERTS, D. W. & PAULSEN, K. D. 2011. Cortical surface strain estimation using stereovision. *Med Image Comput Comput Assist Interv.*

JOLDES, G., WITTEK, A., COUTON, M., WARFIELD, S. & MILLER, K. 2009a. Real-Time Prediction of Brain Shift Using Nonlinear Finite Element Algorithms. *Medical Image Computing and Computer-Assisted Intervention – MICCAI 2009.*

JOLDES, G., WITTEK, A. & MILLER, K. 2009b. Suite of finite element algorithms for accurate computation of soft tissue deformation for surgical simulation. *Medical Image Analysis,* 13**,** 912-919.

JOLDES, G., WITTEK, A., MILLER, K. & MORRISS, L. Year. Realistic and efficient brain-skull interaction model for brain shift computation. *In:* MILLER, K. & NIELSEN, P. M. F., eds.

Computational Biomechanics for Medicine III, International Conference on Medical Image Computing and Computer-Assisted Intervention MICCAI 2008, 2008d New York, USA. Medical Image Computing and Computer-Assisted Intervention, 95-105.

JOLDES, G. R. Year. Cortical surface motion estimation for brain shift prediction. *In:* Computational Biomechanics for Medicine IV (a workshop associated with the International Conference on Medical Image Computing and Computer Assisted Intervention MICCAI 2009). 2009d London. 10.

JOLDES, G. R., WITTEK, A. & MILLER, K. 2009c. Computation of intra-operative brain shift using dynamic relaxation. *Computer Methods in Applied Mechanics and Engineering,* 198**,** 3313-3320.

JOLDES, G. R., WITTEK, A. & MILLER, K. 2009d. Non-locking tetrahedral finite element for surgical simulation. *Communications in Numerical Methods in Engineering,* 25**,** 827-836.

JOLDES, G. R., WITTEK, A. & MILLER, K. 2010. Real-time nonlinear finite element computations on GPU - Application to neurosurgical simulation. *Computer Methods in Applied Mechanics and Engineering,* 199**,** 3305-3314.

JOLDES, G. R., WITTEK, A. & MILLER, K. 2011. An adaptive dynamic relaxation method for solving nonlinear finite element problems. Application to brain shift estimation. *International Journal for Numerical Methods in Biomedical Engineering,* 27**,** 173-185.

KYBIC, J., THEVENAZ, P., NIRKKO, A. & UNSER, M. 2000. Unwarping of unidirectionally distorted EPI images. *IEEE Trans Med Imaging,* 19**,** 80-93.

KYBIC, J. & UNSER, M. 2003. Fast parametric elastic image registration. *Image Processing, IEEE Transactions on,* 12**,** 1427-1442.

LEE, S.-Y., CHWA, K.-Y. & SHIN, S. Y. 1995. Image metamorphosis using snakes and free-form deformations. *Proceedings of the 22nd annual conference on Computer graphics and interactive techniques.* ACM.

LEE, S., WOLBERG, G. & SHIN, S. Y. 1997. Scattered data interpolation with multilevel B-splines. *Visualization and Computer Graphics, IEEE Transactions on,* 3**,** 228-244.

MATTES, D., HAYNOR, D. R., VESSELLE, H., LEWELLEN, T. K. & EUBANK, W. 2003. PET-CT image registration in the chest using free-form deformations. *IEEE Trans Med Imaging,* 22**,** 120-8.

MATTES, D., HAYNOR, D. R., VESSELLE, H., LEWELLYN, T. K. & EUBANK, W. 2001. Nonrigid multimodality image registration. *In:* SONKA, M. & HANSON, K. M. (eds.) *SPIE.*

MEDTRONIC. 2010. *Medtronic Navigation StealthLink Research Portal* [Online]. Available: http://www.na-mic.org/Wiki/index.php/Stealthlink_Protocol [Accessed 21/01/2013 2013].

MILLER, K. & CHINZEI, K. 2002. Mechanical properties of brain tissue in tension. *Journal of Biomechanics,* 35**,** 483-490.

MILLER, K., JOLDES, G., LANCE, D. & WITTEK, A. 2007. Total Lagrangian explicit dynamics finite element algorithm for computing soft tissue deformation. *Communications in Numerical Methods in Engineering,* 23**,** 121-134.

ROHLFING, T., MAURER, C. R., JR., BLUEMKE, D. A. & JACOBS, M. A. 2003. Volume-preserving nonrigid registration of MR breast images using free-form deformation with an incompressibility constraint. *IEEE Trans Med Imaging,* 22**,** 730-41.

RUECKERT, D., SONODA, L. I., HAYES, C., HILL, D. L. G., LEACH, M. O. & HAWKES, D. J. 1999. Nonrigid registration using free-form deformations: application to breast MR images. *Medical Imaging, IEEE Transactions on,* 18**,** 712-721.

RUPRECHT, D. & MULLER, H. 1993. Free form deformation with scattered data interpolation methods. *Geometric modelling.* Springer-Verlag.

SCHNABEL, J. A., RUECKERT, D., QUIST, M., BLACKALL, J. M., CASTELLANO-SMITH, A. D., HARTKENS, T., PENNEY, G. P., HALL, W. A., LIU, H., TRUWIT, C. L., GERRITSEN, F. A., HILL, D. L. G. & HAWKES, D. J. 2001. A Generic Framework for Non-rigid Registration Based on Non-uniform Multi-level Free-Form Deformations. *Proceedings of the 4th International Conference on Medical Image Computing and Computer-Assisted Intervention.* Springer-Verlag.

SINKUS, R., TANTER, M., XYDEAS, T., CATHELINE, S., BERCOFF, J. & FINK, M. 2005. Viscoelastic shear properties of in vivo breast lesions measured by MR elastography. *Magnetic Resonance Imaging,* 23**,** 159-165.

THEVENAZ, P. & UNSER, M. A. 1997. Spline pyramids for intermodal image registration using mutual information. 236-247.

TUSTISON, N. J., AVANTS, B. B., COOK, P. A., ZHENG, Y., EGAN, A., YUSHKEVICH, P. A. & GEE, J. C. 2010. N4ITK: improved N3 bias correction. *IEEE Trans Med Imaging,* 29**,** 1310-20.

WARFIELD, S. K., HAKER, S. J., TALOS, F., KEMPER, C. A., WEISENFELD, N., MEWES, A. U. J., GOLDBERG-ZIMRING, D., ZOU, K. H., WESTIN, C. F., WELLS III, W. M., TEMPANY, C. M. C., GOLBY, A., BLACK, P. M., JOLESZ, F. A., AND KIKINIS, R. 2005. 2005. Capturing Intraoperative Deformations: Research Experience At Brigham and Women's Hospital. *Med Image Anal.,* 9**,** 145-162.

WITTEK, A., HAWKINS, T. & MILLER, K. 2009. On the unimportance of constitutive models in computing brain deformation for image-guided surgery *Biomechanics and Modeling in Mechanobiology,* 8**,** 77-84.

WITTEK, A., JOLDES, G., COUTON, M., WARFIELD, S. K. & MILLER, K. 2010. Patient-specific non-linear finite element modelling for predicting soft organ deformation in real-time; Application to non-rigid neuroimage registration. *Progress in Biophysics and Molecular Biology*, 103**,** 292 - 303.

WITTEK, A., MILLER, K., KIKINIS, R. & WARFIELD, S. K. 2007. Patient-specific model of brain deformation: Application to medical image registration. *Journal of Biomechanics,* 40**,** 919-929.

ZHAO, C., SHI, W. & DENG, Y. 2005. A new Hausdorff distance for image matching. *Pattern Recognition Letters,* 26**,** 581-586.